Research Article
pISSN 1225-6161 • eISSN 2287-9307
Korean Journal of Remote Sensing 2025, 41(3), 525-535
https://doi.org/10.7780/kjrs.2025.41.3.3

Korean Journal of Remote Sensing
KJRS

Application of Change Detection Using Machine Learning Classification Scheme in Google Earth Engine with High-Resolution Satellite Imagery

Jeonghee Lee[1], Kwangseob Kim[2], Kiwon Lee[3]*

[1]Master Student, Department of Applied Convergence Security, Hansung University, Seoul, Republic of Korea
[2]Assistant Professor, Department of Computer Software, Kyungmin University, Uijeongbu, Republic of Korea
[3]Professor, Information System Track, Hansung University, Seoul, Republic of Korea

Abstract: The use of machine learning algorithms provided by the Google Earth Engine (GEE) platform has been increasingly adopted. This study applied the Random Forest (RF) algorithm using both Sentinel-1/2 imagery provided by GEE and high-resolution CAS500-1 imagery to generate Land Use and Land Cover (LULC) classification maps. Based on these maps, a detailed change detection analysis was conducted between the two time points. The study area is Osong-myeon, Pyeongtaek City, Gyeonggi Province, Korea, and two satellite images from November 2022 and November 2023 were used. Three combinations of input datasets were tested for LULC classification: Sentinel-1/2, CAS500-1, and the Normalized Difference Vegetation Index (NDVI) of Sentinel-2. Classification accuracy and Kappa coefficients were reported for each case. The combination of Sentinel-1/2, CAS500-1, and NDVI was used for the change detection analysis. The results showed that 79.01% of the vegetation zone remained unchanged, while 30.10% of the bare zone originated from previously vegetated areas. Additionally, 21.66% of the forest zone in 2023 had newly converted from the bare zone compared to 2022. This study presents the feasibility of high-resolution imagery for precise LULC classification and change detection. It highlights the practical value of the GEE platform in environmental monitoring in a small area.

Keywords: Google Earth Engine, CAS500-1, Change detection, Random forest, Image classification

Received: May 21, 2025
Revised: June 10, 2025
Accepted: June 23, 2025
Published: June 30, 2025

Corresponding author:
Kiwon Lee
E-mail: kilee@hansung.ac.kr

1. Introduction

Google Earth Engine (GEE) is a cloud-based platform for satellite image processing that offers access to petabyte-scale datasets, image processing tools, and machine learning algorithms. This platform enables global users to monitor and analyze Earth's environment efficiently (Amani et al., 2020; Yang et al., 2022). According to Tamiminia et al. (2020), GEE has been widely applied in agriculture, water resource management, wildfire monitoring, and urban analysis. Despite its strengths in processing speed and data accessibility, limitations remain, particularly in its support for high-resolution data and deep learning capabilities.

This study focuses on detecting Land Use and Land Cover (LULC) changes using multi-temporal classification results generated on the GEE platform. Nasiri et al. (2022) applied a seasonal composite approach to classify LULC using Landsat-8 and Sentinel-2 data within GEE, reporting higher classification accuracy with Sentinel-2 imagery. Similarly, Mangkhaseum and Hanazawa (2022) demonstrated the effectiveness of the GEE's Random Forest (RF) algorithm in LULC classification, while Aryal et al. (2023) utilized GEE's machine learning tools to compare Artificial Neural Networks, the Naive Bayes scheme, and the RF algorithms. Among these, the RF algorithm achieved the highest accuracy, whereas the performance of neural networks varied significantly depending on the volume of training data.

Tesfaye et al. (2024) analyzed 30 years of LULC changes in an Ethiopian watershed using Landsat imagery. They found that classification accuracy improves when integrating auxiliary geographic variables such as Normalized Difference Vegetation Index (NDVI), normalized water index, elevation, and slope. Pande et al. (2024) assessed LULC changes in India using Landsat-8 and found that increasing the number of decision trees in the RF model enhanced classification performance. Amindin et al. (2024) evaluated ecosystem stability in response to LULC changes using Landsat data alongside terrain and climate variables. Ahmed et al. (2024) reported that vegetation and water bodies expanded over 20 years in Germany, while urban areas declined, based on Landsat-7 and Landsat-9 imagery. Zhao et al. (2024) compared multiple machine-learning algorithms provided by GEE and confirmed that the RF algorithm consistently outperformed the others regarding classification accuracy.

Lee et al. (2024a, 2024b) applied GEE to analyze LULC classification accuracy using multi-sensor data, including high-resolution satellite imagery. They showed that increasing the diversity and quantity of imagery leads to better classification performance. Savitha et al. (2025) conducted periodic crop classification using Sentinel-2 data. They compared four algorithms: the RF algorithm, Support Vector Machine (SVM), Gradient Tree Boosting (GTB), and Classification and Regression Tree (CART), finding the RF algorithm to yield the best results.

Meanwhile, Cheng et al. (2024) reviewed advancements in change detection techniques over the past decade, highlighting the growing adoption of deep learning approaches to address challenges such as image quality degradation, noise, illumination differences, and complex terrain. They identified future research directions, including solutions for limited training data, improved processing efficiency, and the development of novel models. Jiang et al. (2024) conducted a comprehensive analysis of change detection methods that utilize multi-sensor and diverse remote sensing data, suggesting that integrating high-resolution imagery, multi-sensor fusion techniques, and large-scale artificial intelligence (AI) models will play an essential role in future research.

The motivation and goal of this study are to present the results generated by integrating high-resolution satellite imagery with the GEE platform, which has traditionally been used for large-scale, multi-temporal land cover change detection, applying machine learning algorithms that have been reported to yield high accuracy in various cases. Therefore, this study does not include a comparative analysis of the accuracy of different machine learning or deep learning algorithms. This approach is applied to a small-scale, mixed urban-rural area to assess its effectiveness in capturing more detailed changes.

In this study, we applied externally sourced high-resolution satellite imagery, specifically CAS500-1, to the GEE platform and combined it with Sentinel-1 and Sentinel-2 data. Using GEE's machine learning algorithms, particularly the RF classifier, which has been widely validated in previous studies, we performed LULC classification and conducted object-based, fine-scale change detection. The study area is Pyeongtaek City, Gyeonggi Province, South Korea.

2. Materials and Methods

2.1. Research Scheme

Fig. 1 provides a schematic overview of the data processing workflow and the overall research framework used in this study. The analysis was conducted within the GEE platform, which served as the primary data handling and computation environment.

Generally, when combining heterogeneous sensor imagery such as Sentinel-1 and Sentinel-2, scale adjustments are needed due to differences in the units and value ranges of the datasets, so that the model can interpret each variable on an equal basis. However, since the RF algorithm is based on a tree structure, it is known to be largely unaffected by feature scale (Scornet et al., 2015). Therefore, this scheme can be considered an “off-the-shelf” model that can be applied without preprocessing steps such as band-wise scaling or feature-level normalization. Meanwhile, spatial alignment becomes more critical when the study area is relatively small. In this study, the imagery used was confirmed to be well-aligned based on actual geographic coordinates.

The satellite imagery used for analysis includes Sentinel-1 Ground Range Detected (GRD) SAR data and Sentinel-2 surface reflectance imagery, both available through GEE. In addition, high-resolution CAS500-1 imagery was employed. The CAS500-1 data were externally sourced and manually uploaded to GEE, after which the spatial extent was clipped to match the study area, and necessary preprocessing steps were applied.

Given that the objective of this study is to perform fine-scale image classification based on high-resolution data, the Sentinel-1 and Sentinel-2 images were resampled to align with the spatial resolution of the CAS500-1 imagery. The NDVI was calculated directly from the Sentinel-2 surface reflectance data and used as an input feature for classification.

Two separate LULC classification maps were produced for the

https://doi.org/10.7780/kjrs.2025.41.3.3

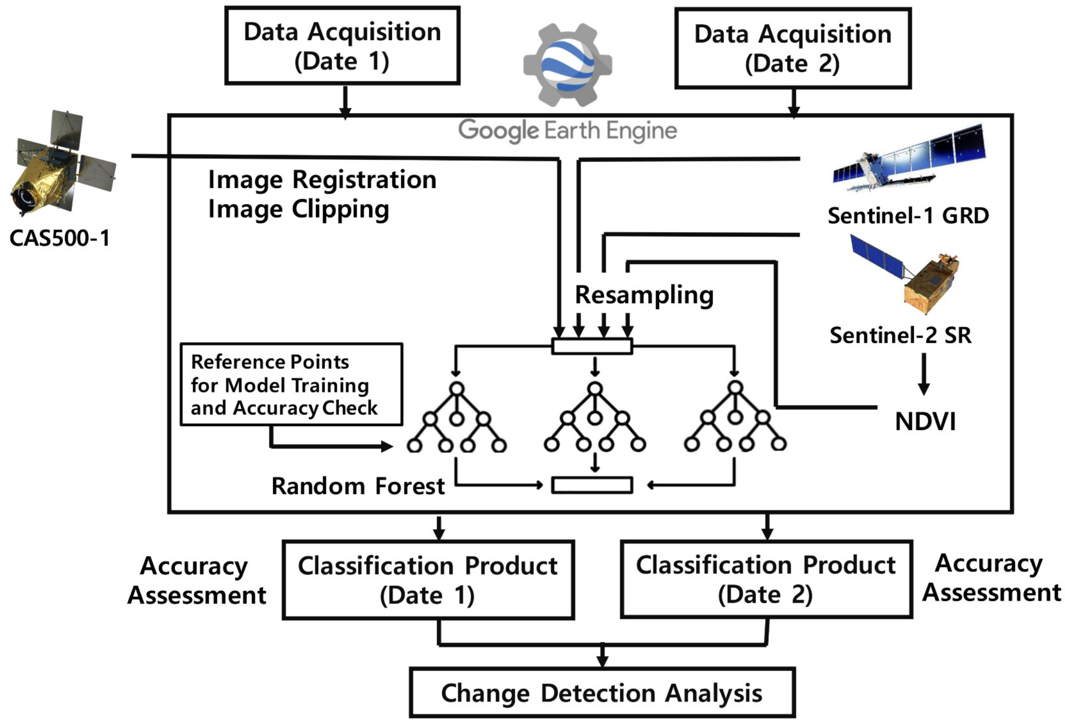

Fig. 1. Workflow using Sentinel-1 and Sentinel-2 images in the Google Earth Engine (GEE), with external data of the CAS500-1 image.

years 2022 and 2023. These were then used to carry out a change detection analysis. We employed the RF algorithm available in GEE to perform the classification. Three experimental setups were designed based on the composition of input data: (1) CAS500-1 imagery alone, (2) a combination of CAS500-1 with Sentinel-1 and Sentinel-2 imagery, and (3) the above combination supplemented with NDVI data. After evaluating classification accuracy for each setup, the change detection analysis was conducted based on the results that achieved the highest accuracy.

2.2. Study Area and Applied Data

The study area is located in Osong-myeon, a township in Pyeongtaek City, Gyeonggi Province, covering approximately 5.1 × 5.5 km (Fig. 2). This region lies adjacent to the western coastline of Korea and is characterized by low elevation and relatively flat terrain, which has fostered the development of the Pyeongtaek Plain, an area well suited for agriculture. In the northwestern part of the study area is Obong Mountain, a hill with an elevation of approximately 110 meters. Gently sloping hills are also found along the eastern and southeastern boundaries. Within the area, two streams, Anseongcheon and Jinwicheon, flow through, with alluvial plains forming along their courses.

For the land cover classification, grasslands, including natural grass, pasture, and managed lawns, and croplands such as paddy fields and cultivated farmland were grouped and classified as a single vegetation zone. The water zone includes rivers, ponds, wetlands, and small streams. The bare zone refers to areas with little to no vegetation where the ground surface is exposed, such as barren patches within grasslands, farmlands, or forested areas. The forest zone encompasses both natural forests and areas of afforestation. The road category includes all types of roads, such as highways, national and local roads, forest roads, farm tracks, and even bridges. Areas that do not fall under these five categories

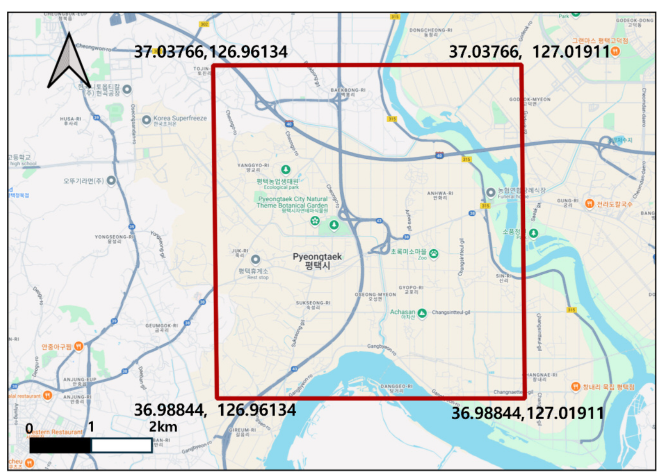

Fig. 2. The study area with geographic location on the Google map.

were labeled as the unclassified zone.

For training and validation of the RF algorithm, the relatively small size of the study area and the distinct surface characteristics of each land cover type allowed for a balanced sampling strategy. A total of 100 training points and 25 validation points were selected for each class, resulting in a dataset of 750 reference samples used in the classification process. The validation points were independently and randomly selected from areas that do not overlap with the training points. In GEE's machine learning, the number of training and validation points is typically determined based on the spatial extent and characteristics of the study area, as well as the number of target classes to be extracted. For example, Abdi (2024) assigned 100 points per class to examine the interrelationships among different GEE machine learning algorithms.

Fig. 3 presents the CAS500-1 satellite imagery used in this study. Fig. 3(a) corresponds to data acquired on November 26, 2022, while Fig. 3(b) shows imagery from November 28, 2023. Fig. 4 displays Sentinel satellite imagery provided by GEE. Figs. 4(a) and 4(b) are Sentinel-2 images captured on November 18,

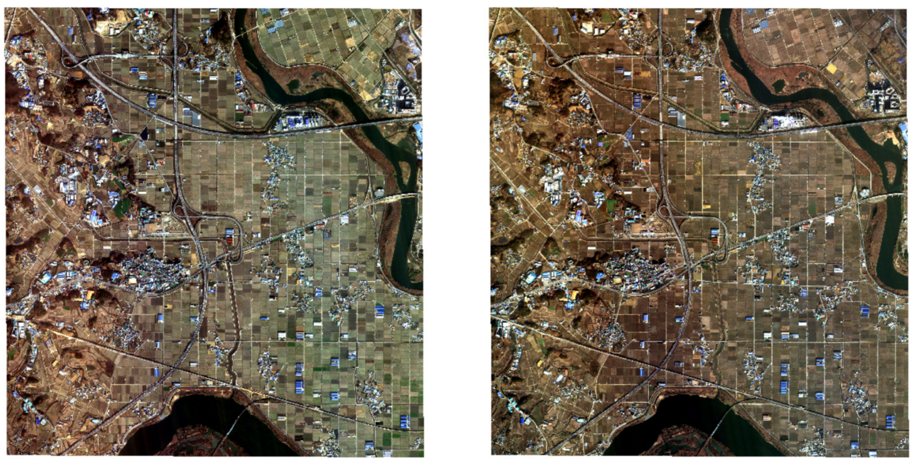

(a) (b)

Fig. 3. True color composite image of CAS500-1: (a) Nov. 26, 2022, and (b) Nov. 28, 2023.

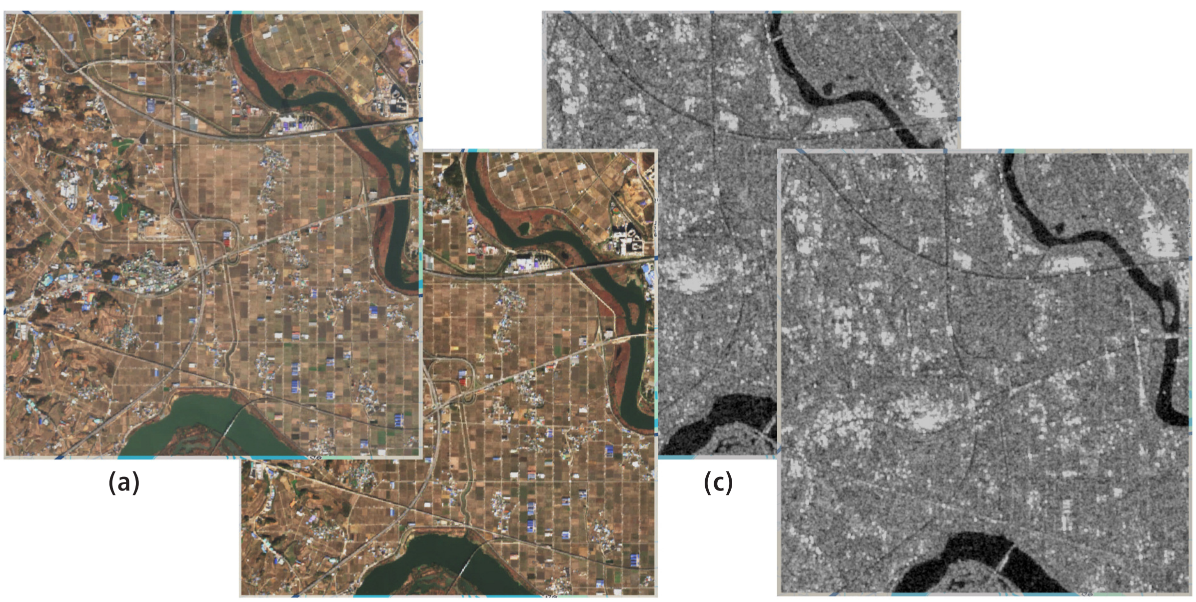

(a) (c)

(b) (d)

Fig. 4. Sentinel images on the Google Earth Engine platform: (a) Sentinel 2 on Nov. 18, 2022, (b) Sentinel 2 on Nov. 13, 2023, (c) Sentinel 1 on Nov. 14, 2022, and (d) Sentinel 1 on Nov. 9, 2023.

https://doi.org/10.7780/kjrs.2025.41.3.3

Table 1. Argument and applied data for the RF scheme in GEE

Argument name	Details	Applied value
numberOfTrees	The number of decision trees to create	100
variablesPerSplit	The number of variables per split	6
minLeafPopulation	Only create nodes whose training set contains at least this many points	1
bagFraction	The fraction of input to bag per tree	0.5
maxNodes	The maximum number of leaf nodes in each tree	1,000
seed	The randomization seed	0

2022, and November 13, 2023, respectively, while Figs. 4(c) and 4(d) are Sentinel-1 images acquired on November 14, 2022, and November 9, 2023.

CAS500-1 and Sentinel-2 images were composed using the Red, Green, Blue, and Near-Infrared (NIR) bands. For Sentinel-1, GRD imagery was used based on VV and VH polarizations, which had been georeferenced to match the terrestrial coordinate system. In the GEE platform, Sentinel-1 GRD imagery is provided in an Analysis-Ready Data (ARD) format (Mullissa et al., 2021).

Since the CAS500-1 imagery used in this study was acquired under nearly cloud-free conditions and provided as Level 2G, offering accurate georeferencing through terrain distortion correction and including basic radiometric preprocessing, it was assumed that spectral comparability with Sentinel-2 surface reflectance data would not be significantly affected. Therefore, additional atmospheric correction was not applied. Surface reflectance data adjusted under the same correction scheme could contribute to some improvement in classification accuracy.

While the CAS500-1 images from the two dates differ by only two days, the Sentinel images show a temporal gap of more than ten days between acquisition dates for each respective year. Although November is generally a stable period with minimal rainfall or vegetation change, these discrepancies in acquisition dates could still introduce potential errors in classification and change detection analyses.

3. Results and Discussion

In this study, LULC classification was performed using the RF algorithm under three different experimental conditions. The first condition utilized only CAS500-1 imagery; the second combined CAS500-1 with Sentinel-1 and Sentinel-2 data; and the third incorporated NDVI data in addition to the combined imagery.

GEE provides the ee.Classifier.smileRandomForest method, which requires six arguments for the RF algorithm (https://developers.google.com/earth-engine/apidocs/ee-classifier-smilerandomforest). The details and values applied to each of these six arguments are presented in Table 1. The same parameter values for the RF algorithm were applied to both the 2022 and 2023 datasets, thereby eliminating the influence of parameter variation on the results.

Fig. 5 presents the classification results for 2022 and 2023 using only CAS500-1 imagery, along with the corresponding class-based confusion matrices (in percentages). Fig. 6 shows the results obtained from the combination of CAS500-1 and Sentinel-1/2 imagery, while Fig. 7 displays the results when NDVI was additionally incorporated, including the related confusion matrices.

When using only the CAS500-1 imagery, the vegetation zone achieved the highest classification accuracy in 2022, whereas the unclassified zone showed the lowest. A similar trend was observed in 2023: the unclassified zone had the lowest accuracy, while the water zone achieved the highest. In the case of combining CAS500-1 with Sentinel-1/2 imagery, the vegetation zone again showed the highest accuracy in 2022, and the unclassified zone remained the lowest. However, in 2023, the vegetation zone achieved perfect classification accuracy (100%), while the bare zone showed the lowest performance. These patterns were consistently observed even when NDVI data were included.

Fig. 8 presents the overall accuracy and Kappa coefficient for the 2022 classification experiments, while Fig. 9 provides the corresponding metrics for the 2023 results. In 2022, the overall accuracy and Kappa coefficient of the land cover classification results slightly increased from 92.0 to 94.0 and from 0.90 to 0.93, respectively, when NDVI was included. In contrast, for 2023, these metrics remained almost the same, showing only a minimal change from 90.7 to 90.0 for overall accuracy and from 0.89 to 0.88 for the Kappa coefficient. This may be due to the characteristics of the study area, which is a mixed urban-rural

	Water Zone	Forest Zone	Bare Zone	Veg. Zone	Road	Unclassified
Water Zone	**96**	4	0	0	0	0
Forest Zone	0	**76**	24	0	0	0
Bare Zone	0	16	**84**	0	0	0
Veg. Zone	0	0	8	**100**	4	0
Road	0	0	0	2	**86**	12
Unclassified	0	4	4	4	16	**72**

	Water Zone	Forest Zone	Bare Zone	Veg. Zone	Road	Unclassified
Water Zone	**96**	4	0	0	0	0
Forest Zone	0	**92**	8	0	0	0
Bare Zone	0	4	**84**	12	0	0
Veg. Zone	0	8	4	**84**	0	4
Road	4	0	0	4	**84**	8
Unclassified	0	4	4	8	8	**76**

(a) (b)

Fig. 5. The confusion matrix (%) and classification result using external data: (a) CAS500-1 image on Nov. 26, 2022, and (b) CAS500-1 image on Nov. 28, 2023.

	Water Zone	Forest Zone	Bare Zone	Veg. Zone	Road	Unclassified
Water Zone	**96**	4	0	0	0	0
Forest Zone	0	**84**	16	0	0	0
Bare Zone	0	0	**100**	0	0	0
Veg. Zone	0	0	8	**100**	0	0
Road	0	0	0	0	**96**	4
Unclassified	0	0	4	4	16	**76**

	Water Zone	Forest Zone	Bare Zone	Veg. Zone	Road	Unclassified
Water Zone	**96**	4	0	0	0	0
Forest Zone	0	**92**	4	4	0	0
Bare Zone	0	4	**80**	16	0	0
Veg. Zone	0	0	0	**100**	0	0
Road	0	0	0	8	**92**	0
Unclassified	0	0	16	0	0	**84**

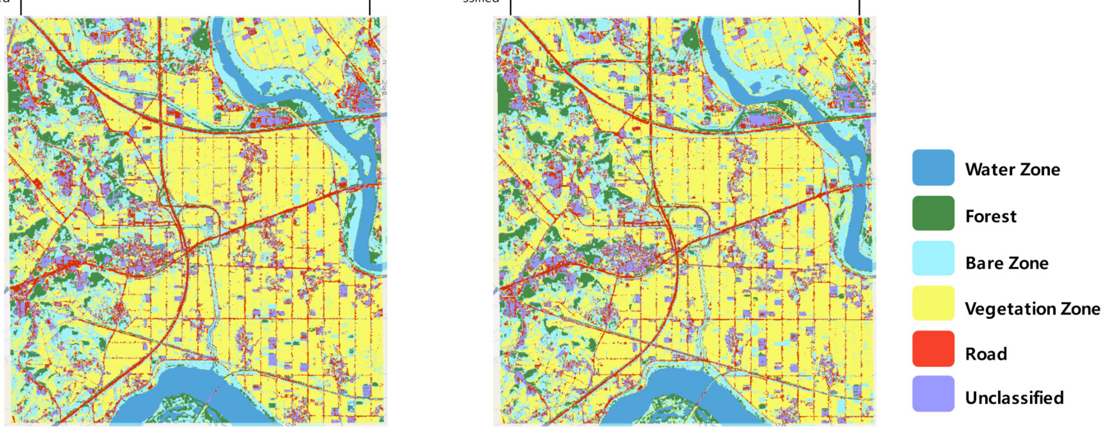

(a) (b)

Fig. 6. The confusion matrix(%) and classification result: (a) Sentinel-1/2 and CAS500-1 image in 2022, and (b) Sentinel-1/2 and CAS500-1 in 2023.

https://doi.org/10.7780/kjrs.2025.41.3.3

	Water Zone	Forest Zone	Bare Zone	Veg. Zone	Road	Unclassified
Water Zone	**96**	4	0	0	0	0
Forest Zone	0	**92**	8	0	0	0
Bare Zone	0	0	**100**	0	0	0
Veg. Zone	0	0	0	**100**	0	0
Road	0	0	0	4	**96**	0
Unclassified	0	4	0	4	12	**80**

	Water Zone	Forest Zone	Bare Zone	Veg. Zone	Road	Unclassified
Water Zone	**96**	4	0	0	0	0
Forest Zone	0	**88**	8	4	0	0
Bare Zone	0	4	**80**	16	0	0
Veg. Zone	0	0	0	**100**	0	0
Road	0	0	4	12	**84**	0
Unclassified	0	0	0	4	4	**92**

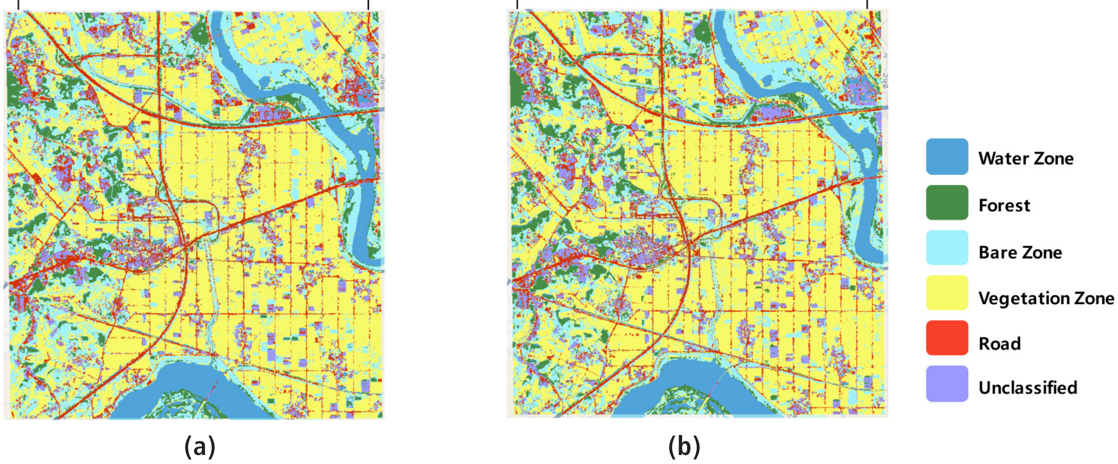

Fig. 7. The confusion matrix(%) and classification result: (a) Sentinel-1/2, NDVI of Sentinel-2 and CAS500-1 image in 2022, and (b) Sentinel-1/2, NDVI of Sentinel-2 and CAS500-1 in 2023.

region where even short-term changes within a year can significantly impact vegetation-related features. However, since the classification results did not show a significant increase or decrease, the impact on the overall change detection analysis is limited.

The applicability and relevance of using NDVI can be preliminarily assessed through a correlation analysis with Sentinel-2 surface reflectance imagery. However, this study did not conduct a separate analysis of variable correlation or importance; instead, it aimed to directly compare classification results with and without the inclusion of NDVI. In the case of the 2022 imagery, the result in Fig. 8(b) showed that excluding NDVI yielded an Overall Accuracy (OA) of 92.0% and a Kappa coefficient of 0.90,

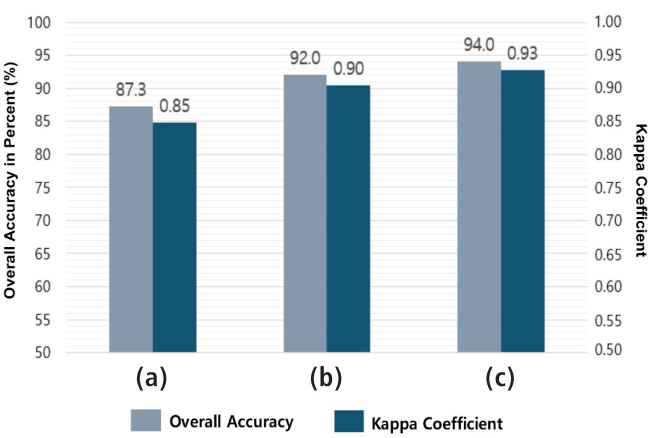

Fig. 8. Overall accuracy and Kappa coefficient regarding classification results using multiple image sets in 2022: (a) CAS500-1 image, (b) Sentinel-1/2 and CAS500-1 image, and (c) Sentinel-1/2, NDVI of Sentinel-2, and CAS500-1 image.

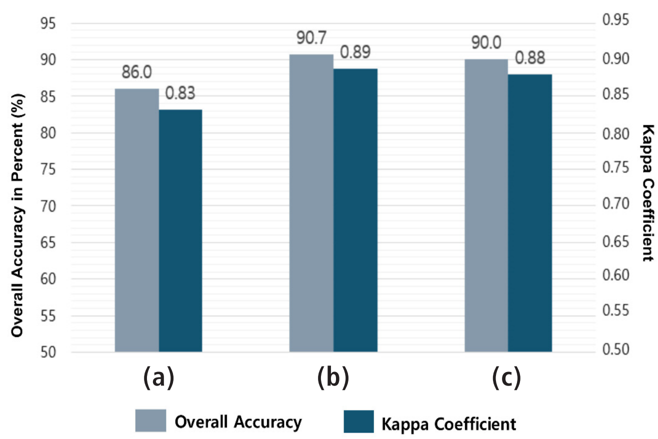

Fig. 9. Overall accuracy and Kappa coefficient regarding classification results using multiple image sets in 2023: (a) CAS500-1 image, (b) Sentinel-1/2 and CAS500-1 image, and (c) Sentinel-1/2, NDVI of Sentinel-2, and CAS500-1 image.

while the result in Fig. 8(c) including NDVI improved the OA to 94.0% and the Kappa to 0.93. This suggests that NDVI slightly enhanced the classification by better representing the widespread vegetation distribution in the study area. In contrast, the 2023 results in Figs. 9(b) and 9(c) showed minimal difference: OA changed from 90.7% to 90.0%, and the Kappa from 0.89 to 0.88. Therefore, in this study, NDVI did not appear to exert a dominant influence on the classification results, nor did it seem to play a reinforcing role by overlapping with other variables.

Fig. 10 presents the results of the change detection analysis based on the 2022 and 2023 LULC classification maps (Fig. 7a, b), which were generated using the combination of Sentinel-1/2 imagery, CAS500-1 imagery, and NDVI as the input set that yielded the highest classification accuracy. In this analysis, the 2023 classification map was used as the reference, and each region was traced back to identify its corresponding class in 2022. Based on this, a total of 36 sub-classes were defined by mapping the transitions between classes across the two time points. For instance, areas classified as vegetation zones in 2023 were further categorized based on whether they belonged to water, forest, vegetation, bare, road, or unclassified zones in 2022. This method was applied to all major class combinations, resulting in 36 distinct sub-classes.

Fig. 10(a) illustrates only the areas where actual changes

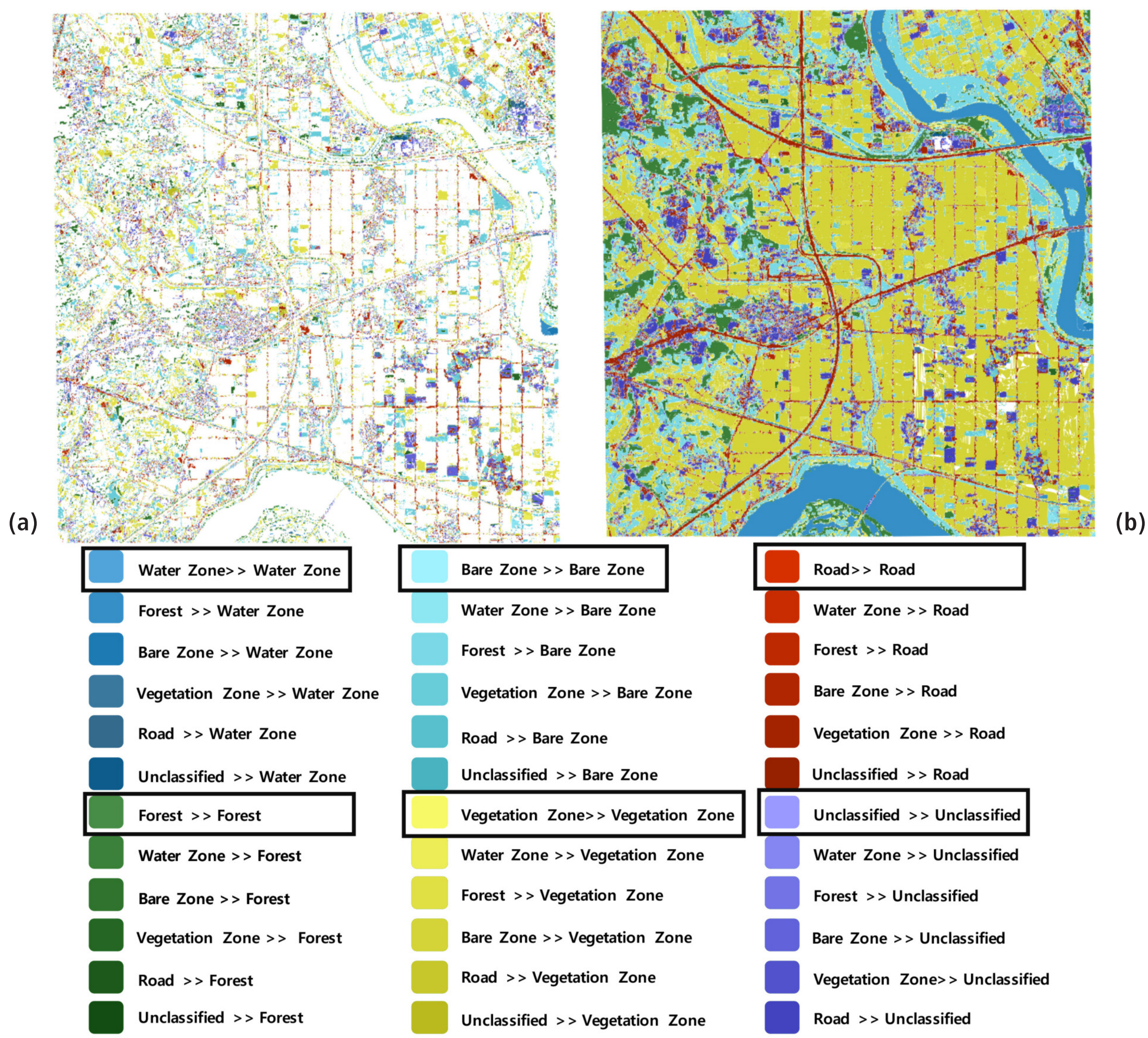

Fig. 10. Change detection by classification results using Sentinel-1/2, NDVI of Sentinel-2, and CAS500-1 image between the two-point date from November 2022 to November 2023: (a) changed areas in each of the classification results and (b) both changed and unchanged areas in the classification results.

https://doi.org/10.7780/kjrs.2025.41.3.3

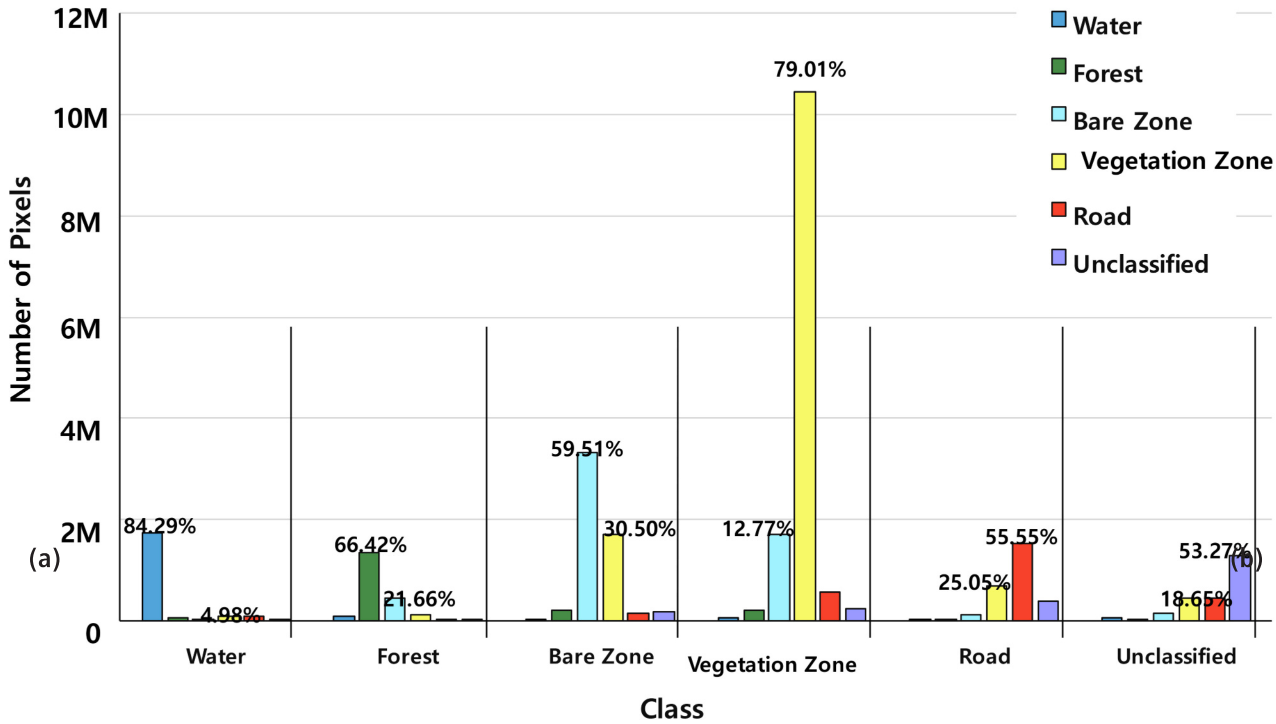

Fig. 11. Object-wise distribution of classification results using Sentinel-1/2, Sentinel-2 NDVI, and CAS500-1 imagery between the two-point date from November 2022 to November 2023.

occurred between the two periods, while Fig. 10(b) shows the spatial distribution of all 36 sub-classes, including unchanged areas. Fig. 11 provides a table summarizing the area of each sub-class in terms of pixel count, based on the change detection results shown in Fig. 10. According to the analysis, 84.29% of the areas classified as water zone in 2023 remained in the same category as in 2022. In the case of the forest zone, 66.42% remained unchanged, while 21.66% had previously been classified as bare zone. The bare zone retained 59.51% of its area, while 30.10% had transitioned from the vegetation zone. For the vegetation zone, which occupied the most significant area, 79.01% remained unchanged, while 12.77% was found to have been converted from the bare zone. Meanwhile, road and unclassified zones maintained 55.55% and 53.27% of their areas, respectively. Among these, 25.05% of the road zone and 18.65% of the unclassified zone were newly converted from the vegetation zone.

4. Conclusions

Change detection studies using satellite imagery have traditionally focused on broad regions over extended periods, primarily relying on medium- to low-resolution imagery. However, many case studies have utilized the GEE platform's satellite datasets and processing capabilities in recent years. In particular, studies that use high-resolution imagery within GEE to analyze detailed object-level changes over short timeframes, typically within one year and in relatively small areas, are emerging as an essential research direction, highlighting the synergic effect between high-resolution data and cloud-based processing platforms.

This study used the GEE platform to conduct LULC classification and change detection experiments for the Osong-myeon area of Pyeongtaek City, located in Gyeonggi Province. A combination of high-resolution CAS500-1 imagery, Sentinel-1/2 imagery, and NDVI was employed as input data. The RF algorithm was applied for classification. The change detection results revealed that 79.01% of the vegetation zone remained unchanged, while 30.10% of the vegetation zone had transitioned into a bare zone. Additionally, 21.66% of the forest zone originated from areas previously classified as bare zones, suggesting ongoing greening in those areas.

These findings offer foundational insights into the spatiotemporal dynamics among vegetation, exposed land, and forest, and demonstrate that high-resolution imagery such as CAS500-1 can effectively detect subtle changes. Therefore, this study validates the applicability of machine learning algorithms for LULC analysis within the GEE environment and highlights the potential for expanding precise environmental monitoring and change detection research using high-resolution satellite imagery.

Acknowledgments

This research was financially supported by Hansung University.

Conflict of Interest

No potential conflict of interest relevant to this article was reported.

References

Abdi, A. M., 2020. Land cover and land use classification performance of machine learning algorithms in a boreal landscape using Sentinel-2 data, *GIScience & Remote Sensing, 57*(1), 1–20. https://doi.org/10.1080/15481603.2019.1650447

Ahmed, R., Zafor, M. A., and Trachte, K., 2024. Land-use and land-cover changes in Cottbus city and Spree-Neisse district, Germany, in the last two decades: A study using remote sensing data and Google Earth Engine. *Remote Sensing, 16*(15), 2773. https://doi.org/10.3390/rs16152773

Amani, M., Ghorbanian, A., Ahmadi, S. A., Kakooei, M., Moghimi, A., Mirmazloumi, S. M., et al., 2020. Google Earth Engine cloud computing platform for remote sensing big data applications: A comprehensive review. *IEEE Journal of Selected Topics in Applied Earth Observations and Remote Sensing, 13*, 5326–5350. https://doi.org/10.1109/JSTARS.2020.3021052

Amindin, A., Siamian, N., Kariminejad, N., Clague, J. J., and Pourghasemi, H. R., 2024. An integrated GEE and machine learning framework for detecting ecological stability under land use/land cover changes. *Global Ecology and Conservation, 53*, e03010. https://doi.org/10.1016/j.gecco.2024.e03010

Aryal, J., Sitaula, C., and Frery, A. C., 2023. Land use and land cover (LULC) performance modeling using machine learning algorithms: A case study of the city of Melbourne, Australia. *Scientific Reports, 13*, 13510, https://doi.org/10.1038/s41598-023-40564-0

Cheng, G., Huang, Y., Li, X., Lyu, S., Xu, Z., Zhao, H., Zhao, Q., and Xiang, S., 2024. Change detection methods for remote sensing in the last decade: A comprehensive review. *Remote Sensing, 16*, 2355. https://doi.org/10.3390/rs16132355

Jiang, W., Sun, Y., Lei, L., Kuang, G., and Ji, K., 2024. Change detection of multisource remote sensing images: A review. *International Journal of Digital Earth, 17*, 2398051. https://doi.org/10.1080/17538947.2024.2398051

Lee, J., Kim, K., and Lee, K., 2024a. Multi-sensor satellite image classification using random forest algorithm in Google Earth Engine: Application of CAS500-1 image sets. *Korean Journal of Remote Sensing, 40*(5–1), 445–453. https://doi.org/10.7780/kjrs.2024.40.5.1.3

Lee, J., Kim, K., and Lee, K., 2024b. Multi-sensor image classification using the random forest algorithm in Google Earth Engine with KOMPSAT-3/5 and CAS500-1 images. *Remote Sensing, 16*(24), 4622. https://doi.org/10.3390/rs16244622

Mangkhaseum Jr, S., and Hanazawa, A., 2022. Validation of random forest algorithm to monitor land cover classification and change detection using remote sensing data in Google Earth Engine. In *Proceedings of the SPIE 12177, International Workshop on Advanced Imaging Technology 2022*, Hong Kong, China, Apr. 30. https://doi.org/10.1117/12.2626085

Mullissa, A., Vollrath, A., Odongo-Braun, C., Slagter, B., Balling, J., Yaqing Gou, Y., et al., 2021. Sentinel-1 SAR backscatter analysis ready data preparation in Google Earth Engine. *Remote Sensing, 13*(10), 1954. https://doi.org/10.3390/rs13101954

Nasiri, V., Deljouei, A., Moradi, F., Sadeghi, S. M. M., and Borz, S.A., 2022. Land use and land cover mapping using Sentinel-2, Landsat-8 satellite images, and Google Earth Engine: A comparison of two composition methods. *Remote Sensing, 14*, 1977. https://doi.org/10.3390/rs14091977

Pande, C. B., Srivastava, A., Moharir, K. N., Radwan, N., Sidek, L. M., Alshehri, F., Pal, S. C., Tolche, A. D., and Zhran, M., 2024. Characterizing land use/land cover change dynamics by an enhanced random forest machine learning model: A Google Earth Engine implementation. *Environmental Sciences Europe, 36*, 84. https://doi.org/10.1186/s12302-024-00901-0

Savitha, C., and Talari, R., 2025. Evaluating the performance of random forest, support vector machine, gradient tree boost, and CART for improved crop-type monitoring using greenest pixel composite in Google Earth Engine. *Environmental Monitoring and Assessment, 197*(4), 437. https://doi.org/10.1007/s10661-025-13880-3

Scornet, E., Biau, G., and Vert, J.-P., 2015. Consistency of random forests. *The Annals of Statistics, 43*(4), 1716–1741. https://

doi.org/10.1214/15-AOS1321

Tamiminia, H., Salehi, B., Mahdianpari, M., Quackenbush, L., Adeli, S., and Brisco, B., 2020. Google Earth Engine for geo-big data applications: A meta-analysis and systematic review. *ISPRS Journal of Photogrammetry and Remote Sensing, 164*, 152–170. https://doi.org/10.1016/j.isprsjprs.2020.04.001

Tesfaye, W., Elias, E., Warkineh, B., Tekalign, M., and Abebe, G., 2024. Modeling of land use and land cover changes using Google Earth Engine and machine learning approach: Implications for landscape management. *Environmental Systems Research, 13*, 31. https://doi.org/10.1186/s40068-024-00366-3

Yang, L., Driscol, J., Sarigai, S., Wu, Q., Chen, H., and Lippitt, C. D., 2022. Google Earth Engine and artificial intelligence (AI): A comprehensive review. *Remote Sensing, 14*(14), 3253. https://doi.org/10.3390/rs14143253

Zhao, Z., Islam, F., Waseem, L. A., Tariq, A., Nawaz, M., Islam, I. U., et al., 2024. Comparison of three machine learning algorithms using Google Earth Engine for land use land cover classification. *Rangeland Ecology & Management, 92*, 129–137. https://doi.org/10.1016/j.rama.2023.10.007